Published in final edited form as:
Neurosci Lett. 2019 June 21; 704: 57–61. doi:10.1016/j.neulet.2019.03.055.

Functional MRI of the mouse olfactory system

Eric R. Muir[a,b,1], **K.C. Biju**[c,1], **Linlin Cong**[a,d], **William E. Rogers**[a], **Enrique Torres Hernandez**[c], **Timothy Q. Duong**[a,b,e], **Robert A. Clark**[c,e,*]

[a]Research Imaging Institute, UT Health San Antonio, 7703 Floyd Curl Drive, San Antonio, Texas 78229;

[b]Department of Ophthalmology, UT Health San Antonio, 7703 Floyd Curl Drive, San Antonio, Texas 78229;

[c]Department of Medicine, UT Health San Antonio, 7703 Floyd Curl Drive, San Antonio, Texas 78229;

[d]Department of Biomedical Engineering, The University of Texas at San Antonio, One UTSA Circle, San Antonio, Texas 78249;

[e]South Texas Veterans Health Care System, 7400 Merton Minter Blvd, San Antonio, Texas 78229

Abstract

Although olfactory dysfunction is an early warning sign of Alzheimer's and Parkinson's diseases, and is commonly present in a range of other neurodegenerative disorders, the mechanisms for its pathogenesis are not yet clear. Since fMRI allows the mapping of spatial and temporal patterns of activity in multiple brain regions simultaneously, it serves as a powerful tool to study olfactory dysfunction in animal models of neurodegenerative diseases. Nonetheless, there have been no reports to date of mapping odor-induced activation patterns beyond the olfactory bulb to the extended networks of olfactory and limbic archicortex, likely due to the small size of the mouse brain. Therefore, using an 11.7 Tesla magnet and a blood volume-weighted fMRI technique, we mapped the functional neuroanatomy of the mouse olfactory system. Consistent with reports on imaging of the much larger human brain, we mapped activity in regions of the olfactory bulb, as well as olfactory and limbic archicortex. By using two distinct odorants, we further demonstrated odorant-specific activation patterns. Our work thus provides a methodological framework for fMRI studies of olfactory dysfunction in mouse models of neurodegeneration.

1. Introduction

Olfactory dysfunction is one of the earliest symptoms of both Alzheimer's and Parkinson's diseases [1–5], and is present to varying degrees in other neurodegenerative conditions, such as multiple sclerosis, schizophrenia, Huntington's disease, and multiple system atrophy (see Kovács 2004 [4] for full list of neurodegenerative conditions in which olfactory

*To whom correspondence should be addressed: Robert A. Clark, MD, Department of Medicine, UT Health San Antonio, 7703 Floyd Curl Drive, San Antonio, TX 78229-3900, CLARKRA@uthscsa.edu.

[1]Equal contributions

dysfunction is reported). Since olfactory dysfunction can predate the development of other clinical signs of either Alzheimer's or Parkinson's disease by years, or even decades, interest in using olfactory dysfunction as a biomarker for early diagnosis of these two major neurodegenerative diseases has increased dramatically in the past decade. However, a major roadblock in realizing the biomarker potential has been the lack of a clear understanding of the mechanism of this olfactory dysfunction, and its causal relationship to the proteinopathies in these neurodegenerative diseases. Since clinical signs or overt anatomical changes are often absent in very early stages of the diseases, to date, there is no diagnostic method for identifying prodromal patients for mechanistic studies. However, the mechanism of olfactory dysfunction can be effectively explored through the use of animal models, since the neural mechanisms of odor processing in rodents are well understood. Moreover, olfaction is remarkable in the extent to which its neural networks are evolutionarily conserved, with striking similarities between human and mouse in the organization of the olfactory pathways [6].

The purpose of this study was to provide a methodological framework for functional magnetic resonance imaging (fMRI) of the mouse olfactory system. Functional MRI provides an incisive tool to study odor-induced functional changes, even when anatomical changes are limited as in early neurodegenerative conditions. Although some studies have previously explored odor-induced activation patterns in mice using blood oxygen level-dependent (BOLD) fMRI [7, 8], these studies were limited to the olfactory bulb. To our knowledge, there are no reports of fMRI mapping of odor-induced activation patterns in mice beyond the olfactory bulb, even though the extended networks of olfactory and limbic archicortex are thought to play an important role in odor identification and discrimination. Since disease-related pathology can disrupt olfaction at multiple levels, the ability to map the entire central olfactory neural network can provide greater insight into disease-specific mechanisms of olfactory dysfunction. Here, using an 11.7 Tesla magnet and a blood volume-weighted fMRI technique, we demonstrate the feasibility and high sensitivity of detecting odor-induced signals throughout the extensive central olfactory network.

2. Methods

2.1. Animal preparation

The experimental procedures were approved by the local Institutional Animal Care and Use Committee. Animal husbandry was in accordance with the National Institutes of Health Guide for the Care and Use of Laboratory Animals, and Society for Neuroscience Policies on the Use of Animals and Humans in Neuroscience Research. Male C57BL/6J mice (Jackson Laboratory, Bar Harbor, Maine) at 15–30 weeks of age were used. Animals were group-housed with *ad libitum* access to food and water. The room temperature was maintained at 26°C, with a light cycle of 12 hours on/12-hours off. For MRI, animals (n = 10) were anesthetized initially with 2% isoflurane for study preparation. An intravenous (IV) line in the lateral tail vein and an intraperitoneal (IP) line were placed. Animals were placed in a head holder with ear and tooth bars. After preparation, animals were injected with an IP bolus of ketamine and xylazine (100 mg/kg and 2.5 mg/kg, respectively) and isoflurane was discontinued. Supplemental boluses of ketamine were injected IP every 20–30 min for

a rate of 100 mg/kg/hr, and 0.3 mg/kg boluses of supplemental xylazine were injected every 30–60 min, as needed. Heart rate and arterial oxygen saturation were monitored (MouseOx, STARR Life Science Corp., Oakmont, PA); the heart rate was 297 ± 11 beats/minutes and arterial oxygen saturation was 79 ± 4 % (n=10, mean ± SEM) during the fMRI. The rectal temperature was maintained at 37 ± 0.5°C with a feedback-regulated circulating warm water pad. For blood volume weighting, monocrystalline iron oxide nanoparticles (MION, Massachusetts General Hospital, Charlestown, Massachusetts) [9, 10] were injected (20 mg/kg, IV).

2.2. Odor delivery

A custom-made, computer-controlled odor delivery device was designed and synchronized with MRI acquisition. Air was passed over the odorants in sealed vials at a flow rate of 2 l/min and delivered to the animal by a nose cone. Two separate lines were input to the nose cone, one to deliver air during baseline periods and one to deliver odorized air during stimulation periods. A vacuum line connected to the odorant line at the nose cone was automatically opened for 7 seconds at the end of odor stimulation periods to remove the odor. A second vacuum line placed next to the head of the animal was always open to prevent buildup of odor in the MRI scanner bore.

Odorants consisted of isoamyl acetate (IAA; a common odorant with an odor quality of banana), diluted to 5% in mineral oil [11, 12], and female mouse urine collected from 12–25 week old C57BL/6J mice (Jackson Laboratory). Urine (0.12–0.4 ml) was collected directly before MRI was performed and used fresh and undiluted.

2.3. Magnetic resonance imaging

MRI was performed on an 11.7 T magnet with 740 mT/m gradients (Bruker, Billerica, Massachusetts) and with a 1 cm transmit/receive surface coil. Blood volume-weighted fMRI was acquired after MION injection using a 3D FLASH (fast low angle shot) sequence with TE/TR = 3.6/10 ms, temporal resolution of 15 s/image, in-plane phase encoding partial Fourier = 78%, FOV = 12.8 × 12.8 × 12 mm, and matrix = 64 × 64 × 30. The power of the excitation pulse from the surface coil was initially optimized to provide high signal across the brain and a similar power was then used for all animals. Using a midsagittal localizer as a reference, the excited slab was centered on the anterior commissure and then moved anterior by 0.3 mm. Distance of imaging slices relative to the bregma were determined based on the distance from the anterior commissure, which is essentially at the bregma [13], from the midsagittal reference. T_1-weighted anatomical reference images were collected before MION injection similarly, but with TE/TR = 4.7/14 ms and matrix = 128 × 128 × 30. A single fMRI trial consisted of 3 epochs of 3-min air and 2-min odor, followed by a period of 3-min air at the end. Three fMRI trials were performed in each animal. Five to ten minutes were given between trials during which time a supplemental bolus of ketamine and occasional xylazine were given. Stimulation with IAA (n = 4) or urine (n = 6) was performed in separate animals.

2.4. MRI analysis

Image analysis was done using Matlab (MathWorks, Natick, MA), SPM8 (Wellcome Trust Centre for Neuroimaging, University College London, UK), FSL 5.0 (FMRIB, Oxford, UK), and Mango (Research Imaging Institute, University of Texas Health Science Center at San Antonio, TX) software. Time-series MRI data were motion corrected with SPM8, and then the three trials were averaged. For group analysis, all images were linearly co-registered with 12 parameters to the T_1-weighted anatomical reference image from one of the mice using FSL. fMRI data were preprocessed in FSL, including spatial smoothing with a full-width half-max of 2 voxels, and group Z-Scores were calculated. Data were displayed using a Z-Score threshold and a minimum cluster size of 64 voxels.

Region of interest (ROI) analysis was performed by manually aligning the group data with 12 parameters to the 2008 coronal Allen Mouse Brain Atlas (Allen Institute for Brain Science; available from: http://mouse.brain-map.org) [14]. For alignment, a resampled version of the Allen atlas and a fake MRI mouse brain template derived from the atlas were obtained with the JIP Toolkit 3.0 (Massachusetts General Hospital, Boston, MA, www.nitrc.org/projects/jip/) [15]. ROIs of brain regions known to be in the olfactory system and/or that showed strong fMRI activation were drawn manually using the Allen atlas.

3. Results

3.1. Olfactory activation patterns of isoamyl acetate

Group fMRI maps of the olfactory bulb in response to IAA stimulation are shown in Figure 1. In the main olfactory bulb, the strongest activation consistently occurred in two regions, one on the medial and one on the lateral aspect of each bulb. These two regions were confined to the superficial layers of the olfactory bulb, which include the olfactory nerve layer and glomerular layer, and may represent the nearly mirror projections of the olfactory receptor neuron subsets in the nasal olfactory epithelium [16, 17]. Furthermore, the activation patterns were relatively similar in the right and left olfactory bulbs. While IAA elicited strong activation in the main olfactory bulb, no activation was observed in the accessory olfactory bulb.

Interestingly and for the first time, we were able to map odor-induced activity from the entire regions of the primary olfactory cortex, which receive axonal projections from the olfactory bulb, as well as various limbic areas associated with olfactory processing (Fig. 2 and 3). The brain regions that were strongly activated by IAA included the piriform cortex (Pir), olfactory tubercle (OT), areas of the amygdala (COAa and COApl), nucleus of the lateral olfactory tract (NLOT), and the entorhinal cortex (Ent). Moreover, moderate signals were also detected in the anterior olfactory nucleus (AON), lateral orbital area (ORBl), dorsal taenia tecta (TTd), layer 1/2 of the primary motor area (MOp), layer 1/2 of the secondary motor area (MOs), layer 1/2 of the primary somatosensory area (SSp), caudoputamen (CP), dorsal thalamic areas (THd), and hippocampal regions (HIP). Lastly, the pattern of activation was largely symmetrical between the left and right hemispheres.

3.2. Olfactory activation patterns of mouse urine

To test further the sensitivity of fMRI for mapping the entire brain regions associated with odor processing, as well as to determine whether the spatial patterns of activation were odorant-specific, fMRI was also performed using mouse urine as an odorant. Unlike IAA, a relatively simple odorant, mouse urine contains a complex mixture of volatile compounds, including pheromones [8, 18]. As for IAA, mouse urine induced activation in the superficial layers of the main olfactory bulb; however, intense activation was restricted to a single region in the ventrolateral aspect of each olfactory bulb, and it extended more posteriorly than IAA-induced activation (Fig. 1). In addition, modest activation was observed in the accessory olfactory bulb.

Compared with IAA, mouse urine induced strikingly different patterns of activation in the brain (Fig. 2). Intense activation occurred primarily in the dorsal part of the endopiriform nucleus (EPd), prelimbic and infralimbic cortices (PL/ILA), ventral part of the anterior cingulate area (ACAv), posterior region of the piriform cortex, posterior hypothalamus (HY), thalamus (TH), dentate gyrus (DG), and temporal association area (TEa). Moderate levels of activation were also observed in the anterior olfactory nucleus, orbital area, retrosplenial area (RSP), entorhinal area, perirhinal area (PERI), and ectorhinal area (ECT). A striking feature of urine stimulation was the activation of various nuclei in the midbrain (Fig. 2 and 3), whereas no activation was observed in any of the midbrain nuclei with IAA. Moreover and unlike IAA-induced activation, the patterns observed induced by mouse urine were often asymmetric between the left and right hemispheres.

The Z-Scores of major brain regions activated by either IAA or mouse urine are summarized in Table 1.

4. Discussion

Using blood volume-weighted high-resolution functional MRI we demonstrated odorant-induced activation throughout the central olfactory network for the first time in mice. By using two unrelated odorants, IAA and mouse urine, we further showed that the activation patterns were odorant-specific. Although previous fMRI studies of odor-induced activation patterns in mice were limited to the olfactory bulb [7, 8], recent olfactory fMRI studies in rat, which has a larger brain, have reported activation beyond the olfactory bulb to anterior olfactory nucleus and piriform cortex [19–21]. However, compared to the studies in rat [19–21], we observed a more widespread and stronger activation throughout the mouse olfactory neural circuit. Some potential differences compared to previous studies that could account for the more widespread activation in our study include 11.7 T scanner herein vs. 4.7 T or 7 T used previously and the use of MION to enhance the cerebrovascular response, as well as possible differences in imaging coils, imaging sequences, odors and their concentrations, and choice of anesthesia.

Isoamyl acetate and mouse urine both elicited distinct and reproducible patterns of activation in the superficial layers of the olfactory bulb that were largely consistent with previous olfactory fMRI studies in mice [7, 8]. However, urine-induced activation in the accessory olfactory bulb was much less intense in our study, compared with a previous report [8].

This discrepancy may be due to differences in the sex of the animals, as well as in the pheromone signature of the urine samples in the two studies. Female mice were imaged under stimulation with male mouse urine in that study [8], whereas we imaged males stimulated with female urine. Consistent with the sparse activation in the accessory olfactory bulb, we also found that some brain regions in the accessory olfactory network were not activated by urine, including areas of the amygdala, the bed nucleus of the stria terminalis, and the ventral tegmental area. In addition, only sparse activation was observed in the medial preoptic area of the hypothalamus and the nucleus accumbens [22].

Within the brain, IAA induced activation, to varying degrees, in all regions of the olfactory and limbic archicortex involved in olfactory processing [23], whereas mouse urine elicited activation only in limited regions of the olfactory and limbic archicortex. A prominent feature of the urine odor map is the activation of various small nuclei in the thalamic, hypothalamic, and midbrain regions, whereas no activation was observed in any of these areas with IAA. Since these nuclei are very small and MRI does not provide sufficient contrast to distinguish most of them in the mouse brain, even small errors in the alignment between the MRI data and the atlas could confound correct identification. Therefore, we have refrained from making any conclusions about specific nuclei from thalamic, hypothalamic, and midbrain regions. However, it is interesting to note that many of these nuclei are involved in social and reproductive behaviors in mice [24]. Since the accessory olfactory bulb was only sparsely activated by mouse urine, the small nuclei in the thalamic, hypothalamic, and midbrain regions were more likely activated by pheromone signals from the main olfactory bulb. The traditional view has been that the main olfactory bulb processes common odors, while the accessory olfactory bulb processes pheromone signals to mediate specific endocrine, social communication, and reproductive behavioral responses [25, 26]. However, it is now evident that the distinction between the two olfactory systems is not absolute. Instead, responses to pheromones and common odorants exhibit significant overlap between these two systems [8]. Indeed, the main olfactory epithelium, which innervates the main olfactory bulb, contains a subset of olfactory sensory neurons that express a distinct class of molecules called trace amine-associated receptors [27]. These receptors are activated by compounds in mouse urine involved in social communication and reproductive behavior. Moreover, a major olfactory projection pathway originating from a discrete population of olfactory sensory neurons and innervating hypothalamic neurons controlling fertility and reproduction has been identified [24]. Thus, our work provides further support for pheromone reception by the main olfactory epithelium. While the spatial pattern of activation to urine was substantially different than that of activation to IAA, the urine response was also relatively weak and sparse. As such, further studies with more animals are needed to better determine the precise activation pattern due to urine odorant. Studies of sex-related differences as well as reproductive status are also needed to fully elucidate the olfactory network response to pheromones.

In the olfactory bulb both mitral/tufted cells and granule cells express NMDA receptors, and the NMDA receptors play a key role in olfactory processing [28–30]. In the current study, we used ketamine, which is also an NMDA receptor antagonist, as the anesthetic during fMRI. Although we cannot completely exclude the possibility of potential influence of ketamine on the intensity of odor-induced activation, based on the strikingly different

spatial pattern of activation between IAA and urine, it is unlikely that ketamine significantly influenced the overall pattern of activation. This notion receives further support from a recent IAA-induced olfactory fMRI study in rat [20] in which dexmedetomidine (α−2 adrenergic agonist) was used as the anesthetic. The pattern of activation in the olfactory bulb in that study and ours was similar (activation localized primarily in the glomerular layer), indicating that the anesthetic did not have significant effect on the activation pattern in the olfactory bulb. Moreover, it has been reported that the overall dynamic pattern of olfactory bulb oscillations under ketamine/xylazine cocktail resembles that of the awake state in mice, and that this similarity between oscillations in anesthetized and awake states makes ketamine/xylazine cocktails more suitable for studying odor processing in the olfactory bulb [28]. NMDA receptor antagonists has also been shown to influence odor-induce olfactory activation by blocking olfactory adaptation to repeated odor stimulus during fMRI [19]. While, we cannot discern any effect of ketamine on potential olfactory adaptation in the current study, it is unlikely to be an issue. Olfactory adaptation during odor-induced fMRI is detected only with repeated odor stimulation protocols such as 60 or 80 repetitions of 40 second (baseline) + 40 second (stimulation) + 80 second (recovery) for over the period of a 3- [20] or 4-hour [19] fMRI session. In the current study, a single fMRI trial consisted of 3 epochs of 3-minutes air and 2-minutes odor, followed by a period of 3-minutes air at the end, and three fMRI trials were performed for each animal. We did not observe significant adaptation during the 2-minute activation period. This is consistent with a recent study [19] that showed no olfactory adaptation in rat during a prolonged 200 second stimulation using the same odorant (IAA) we used in our study.

In summary, until now it has not been possible to visualize and compare the entire odor map in mice due to technical limitations. However, this study shows that under an 11.7 T magnet the entire olfactory neural circuitry of the mouse brain can be imaged with high signal-to-noise ratio, thus providing a novel methodologic framework for comprehensive investigation of mouse olfactory neural networks in normal and disease states. The significance of these findings is underscored by the fact that sense of smell is among the first casualties of neurodegenerative diseases, such as Alzheimer’s and Parkinson’s. Although interest in using olfaction as a biomarker for these conditions has increased substantially in recent years, the mechanism of olfactory loss and its causal relationship to the pathological hallmarks of these diseases remain unclear. Filling this major knowledge gap in well-defined animal models would significantly inform our understanding of the mechanisms involved in the initiation and progression of the disease pathology, while at the same time providing a rapid and objective assessment of disease risk. The spatiotemporal coding of olfactory stimuli involves an extended network of brain regions. Unlike other neuroscience techniques, fMRI allows simultaneous imaging of the spatial distribution and temporal dynamics of activation in the entire olfactory network *in vivo*. Moreover, fMRI technology makes it possible to study not only disease-related changes in the activation of a particular region, but also its connectivity to other brain regions. Lastly, since the odor maps of IAA stimulation reported in the current study are consistent with those reported in human olfactory fMRI studies [23], data on the functional neuroanatomy of the mouse olfactory system is readily translatable to humans.

Acknowledgments

This work was supported by a Merit Review Grant from the Veterans Health Administration (1 101 BX 003157) and a grant from the William and Ella Owens Medical Research Foundation, both awarded to RAC.

Abbreviations:

ACAv	ventral part of anterior cingulate area
ACB	nucleus accumbens
AOB	accessory olfactory bulb
AON	anterior olfactory nucleus
BOLD	blood oxygen level-dependent
COAa	cortical amygdalar area, anterior part
COApl	cortical amygdalar area, posterior part
CP	caudoputamen
DG	dentate gyrus
ECT	ectorhinal area
Ent	entorhinal cortex
EPd	endopiriform nucleus
fMRI	functional magnetic resonance imaging
GL	glomerular layer
HIP	hippocampus
HY	hypothalamus
IAA	isoamyl acetate
IP	intraperitoneal
IV	intravenous
MB	midbrain
MION	monocrystalline iron oxide nanoparticles
MOp	primary motor area
MOs	secondary motor area
NLOT	nucleus of the lateral olfactory tract
ORBl	lateral orbital area

OT	olfactory tubercle
PERI	perirhinal area
Pir	piriform cortex
PL/ILA	prelimbic and infralimbic cortices
RSP	retrosplenial area
SSp	primary somatosensory area
TEa	temporal association area
TH	thalamus
THd	dorsal thalamic areas
TTd	dorsal taenia tecta

References

[1]. Devanand DP, Lee S, Manly J, Andrews H, Schupf N, Doty RL, Stern Y, Zahodne LB, Louis ED, Mayeux R, Olfactory deficits predict cognitive decline and Alzheimer dementia in an urban community, Neurology, 84 (2015) 182–189. [PubMed: 25471394]

[2]. Kreisl WC, Jin P, Lee S, Dayan ER, Vallabhajosula S, Pelton G, Luchsinger JA, Pradhaban G, Devanand DP, Odor Identification Ability Predicts PET Amyloid Status and Memory Decline in Older Adults, J Alzheimers Dis, 62 (2018) 1759–1766. [PubMed: 29614678]

[3]. Doty RL, Olfactory dysfunction in Parkinson disease, Nat. Rev. Neurol, 8 (2012) 329–339. [PubMed: 22584158]

[4]. Kovacs T, Mechanisms of olfactory dysfunction in aging and neurodegenerative disorders, Ageing Res. Rev, 3 (2004) 215–232. [PubMed: 15177056]

[5]. Wu Y, Le W, Jankovic J, Preclinical biomarkers of Parkinson disease, Arch. Neurol, 68 (2011) 22–30. [PubMed: 21220674]

[6]. Ache BW, Young JM, Olfaction: diverse species, conserved principles, Neuron, 48 (2005) 417–430. [PubMed: 16269360]

[7]. Xu F, Liu N, Kida I, Rothman DL, Hyder F, Shepherd GM, Odor maps of aldehydes and esters revealed by functional MRI in the glomerular layer of the mouse olfactory bulb, Proc Natl Acad Sci U S A, 100 (2003) 11029–11034. [PubMed: 12963819]

[8]. Xu F, Schaefer M, Kida I, Schafer J, Liu N, Rothman DL, Hyder F, Restrepo D, Shepherd GM, Simultaneous activation of mouse main and accessory olfactory bulbs by odors or pheromones, J Comp Neurol, 489 (2005) 491–500. [PubMed: 16025460]

[9]. Kim YR, Huang IJ, Lee SR, Tejima E, Mandeville JB, van Meer MP, Dai G, Choi YW, Dijkhuizen RM, Lo EH, Rosen BR, Measurements of BOLD/CBV ratio show altered fMRI hemodynamics during stroke recovery in rats, J Cereb Blood Flow Metab, 25 (2005) 820–829. [PubMed: 15758949]

[10]. Mandeville JB, Jenkins BG, Chen YC, Choi JK, Kim YR, Belen D, Liu C, Kosofsky BE, Marota JJ, Exogenous contrast agent improves sensitivity of gradient-echo functional magnetic resonance imaging at 9.4 T, Magn Reson Med, 52 (2004) 1272–1281. [PubMed: 15562489]

[11]. Poplawsky AJ, Fukuda M, Murphy M, Kim SG, Layer-Specific fMRI Responses to Excitatory and Inhibitory Neuronal Activities in the Olfactory Bulb, J Neurosci, 35 (2015) 15263–15275. [PubMed: 26586815]

[12]. Poplawsky AJ, Kim SG, Layer-dependent BOLD and CBV-weighted fMRI responses in the rat olfactory bulb, Neuroimage, 91 (2014) 237–251. [PubMed: 24418506]

[13]. Paxinos G, Franklin KBJ, The mouse brain in stereotaxic coordinates, 2 ed., Academic Press, San Diego. 2001.

[14]. Lein ES, Hawrylycz MJ, Ao N, Ayres M, Bensinger A, Bernard A, Boe AF, Boguski MS, Brockway KS, Byrnes EJ, Chen L, Chen L, Chen TM, Chin MC, Chong J, Crook BE, Czaplinska A, Dang CN, Datta S, Dee NR, Desaki AL, Desta T, Diep E, Dolbeare TA, Donelan MJ, Dong HW, Dougherty JG, Duncan BJ, Ebbert AJ, Eichele G, Estin LK, Faber C, Facer BA, Fields R, Fischer SR, Fliss TP, Frensley C, Gates SN, Glattfelder KJ, Halverson KR, Hart MR, Hohmann JG, Howell MP, Jeung DP, Johnson RA, Karr PT, Kawal R, Kidney JM, Knapik RH, Kuan CL, Lake JH, Laramee AR, Larsen KD, Lau C, Lemon TA, Liang AJ, Liu Y, Luong LT, Michaels J, Morgan JJ, Morgan RJ, Mortrud MT, Mosqueda NF, Ng LL, Ng R, Orta GJ, Overly CC, Pak TH, Parry SE, Pathak SD, Pearson OC, Puchalski RB, Riley ZL, Rockett HR, Rowland SA, Royall JJ, Ruiz MJ, Sarno NR, Schaffnit K, Shapovalova NV, Sivisay T, Slaughterbeck CR, Smith SC, Smith KA, Smith BI, Sodt AJ, Stewart NN, Stumpf KR, Sunkin SM, Sutram M, Tam A, Teemer CD, Thaller C, Thompson CL, Varnam LR, Visel A, Whitlock RM, Wohnoutka PE, Wolkey CK, Wong VY, Wood M, Yaylaoglu MB, Young RC, Youngstrom BL, Yuan XF, Zhang B, Zwingman TA, Jones AR, Genome-wide atlas of gene expression in the adult mouse brain, Nature, 445 (2007) 168–176. [PubMed: 17151600]

[15]. Liu CH, Greve DN, Dai G, Marota JJ, Mandeville JB, Remifentanil administration reveals biphasic phMRI temporal responses in rat consistent with dynamic receptor regulation, Neuroimage, 34 (2007) 1042–1053. [PubMed: 17169578]

[16]. Mombaerts P, Wang F, Dulac C, Chao SK, Nemes A, Mendelsohn M, Edmondson J, Axel R, Visualizing an olfactory sensory map, Cell, 87 (1996) 675–686. [PubMed: 8929536]

[17]. Vassar R, Chao SK, Sitcheran R, Nunez JM, Vosshall LB, Axel R, Topographic organization of sensory projections to the olfactory bulb, Cell, 79 (1994) 981–991. [PubMed: 8001145]

[18]. Schwende FJ, Wiesler D, Novotny M, Volatile compounds associated with estrus in mouse urine: potential pheromones, Experientia, 40 (1984) 213–215. [PubMed: 6538143]

[19]. Zhao F, Wang X, Zariwala HA, Uslaner JM, Houghton AK, Evelhoch JL, Hostetler E, Winkelmann CT, Hines CDG, fMRI study of the role of glutamate NMDA receptor in the olfactory adaptation in rats: Insights into cellular and molecular mechanisms of olfactory adaptation, Neuroimage, 149 (2017) 348–360. [PubMed: 28163142]

[20]. Zhao F, Wang X, Zariwala HA, Uslaner JM, Houghton AK, Evelhoch JL, Williams DS, Winkelmann CT, fMRI study of olfaction in the olfactory bulb and high olfactory structures of rats: Insight into their roles in habituation, Neuroimage, 127 (2016) 445–455. [PubMed: 26522425]

[21]. Chen W, Shields J, Huang W, King JA, Female fear: influence of estrus cycle on behavioral response and neuronal activation, Behav Brain Res, 201 (2009) 8–13. [PubMed: 19428610]

[22]. Baum MJ, Sexual differentiation of pheromone processing: links to male-typical mating behavior and partner preference, Horm Behav, 55 (2009) 579–588. [PubMed: 19446074]

[23]. Barresi M, Ciurleo R, Giacoppo S, Foti Cuzzola V, Celi D, Bramanti P, Marino S, Evaluation of olfactory dysfunction in neurodegenerative diseases, J Neurol Sci, 323 (2012) 16–24. [PubMed: 23010543]

[24]. Yoon H, Enquist LW, Dulac C, Olfactory inputs to hypothalamic neurons controlling reproduction and fertility, Cell, 123 (2005) 669–682. [PubMed: 16290037]

[25]. Dulac C, Torello AT, Molecular detection of pheromone signals in mammals: from genes to behaviour, Nat Rev Neurosci, 4 (2003) 551–562. [PubMed: 12838330]

[26]. Meredith M, Vomeronasal, olfactory, hormonal convergence in the brain. Cooperation or coincidence?, Ann N Y Acad Sci, 855 (1998) 349–361. [PubMed: 9929627]

[27]. Liberles SD, Buck LB, A second class of chemosensory receptors in the olfactory epithelium, Nature, 442 (2006) 645–650. [PubMed: 16878137]

[28]. Chery R, Gurden H, Martin C, Anesthetic regimes modulate the temporal dynamics of local field potential in the mouse olfactory bulb, J Neurophysiol, 111 (2014) 908–917. [PubMed: 24285865]

[29]. Lee JH, Wei L, Deveau TC, Gu X, Yu SP, Expression of the NMDA receptor subunit GluN3A (NR3A) in the olfactory system and its regulatory role on olfaction in the adult mouse, Brain Struct Funct, 221 (2016) 3259–3273. [PubMed: 26334321]

[30]. Wilson DA, Sullivan RM, Gall CM, Guthrie KM, NMDA-receptor modulation of lateral inhibition and c-fos expression in olfactory bulb, Brain Res, 719 (1996) 62–71. [PubMed: 8782864]

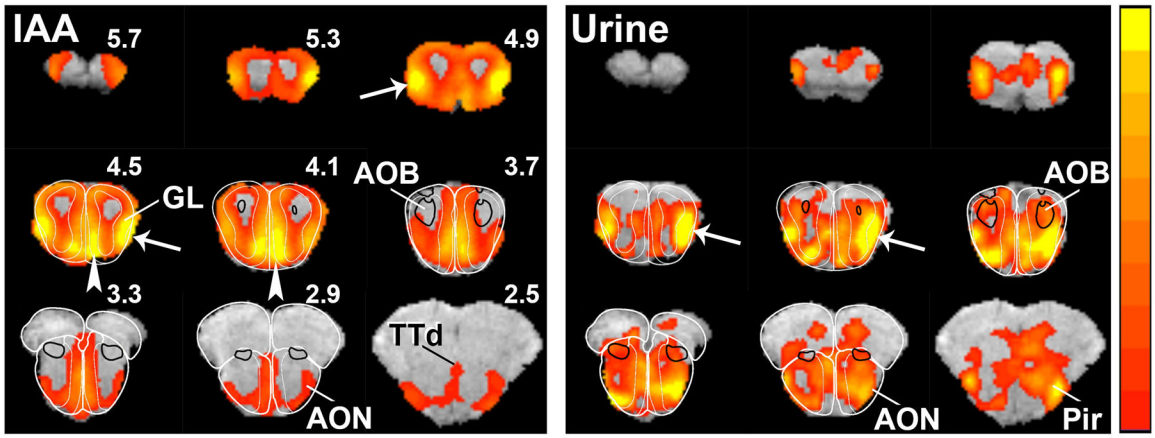

Fig. 1.

Odor maps of isoamyl-acetate (IAA) and urine in the olfactory bulb. Color bar indicates Z-Scores scaled from 5 (red) to 14 (yellow) for IAA and 2.3 (red) to 5 (yellow) for urine. The lower Z-Score thresholds were taken as the median Z-Scores of all voxels in the brain in the slices depicted for each odor activation map. Thus, any voxel with a Z-score less than the median is not shown as activated. The lower Z thresholds of 2.3 and 5 correspond to uncorrected, two-tailed P-values of 0.021 and 6E-7, respectively, and it is applicable to Fig. 2 as well. Arrows and arrowheads indicate activation in the lateral and medial glomerular layers, respectively. Outlines of the olfactory bulb and AOB regions were drawn from the Paxinos and Franklin atlas (G. Paxinos, K.B.J. Franklin, The mouse brain in stereotaxic coordinates, 2 ed., Academic Press, San Diego. 2001). AOB, accessory olfactory bulb; AON, anterior olfactory nucleus; GL, glomerular layer; Pir, piriform cortex; TTd, dorsal taenia tecta.

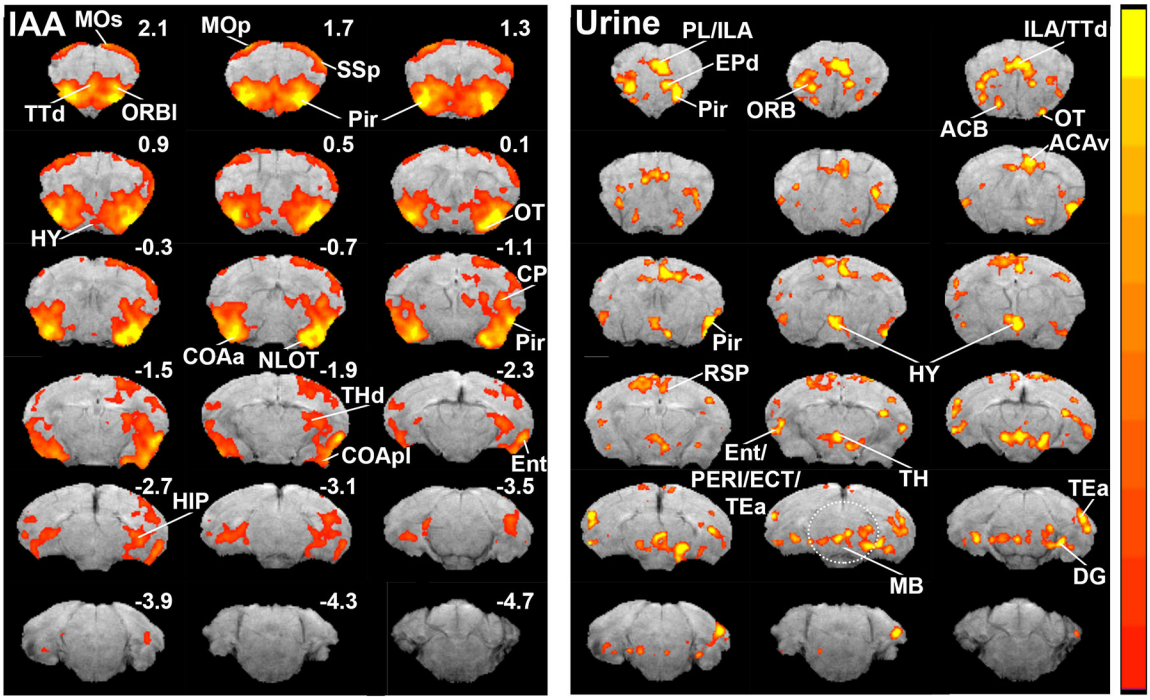

Fig. 2.

Odor maps of isoamyl-acetate (IAA) and urine in the brain. Color bar indicates Z-Scores scaled from 2.3 (red) to 7 (yellow) for IAA and 2.3 (red) to 3.5 (yellow) for urine. ACAv ventral part of anterior cingulate area; ACB, nucleus accumbens; COAa, cortical amygdalar area, anterior part; COApl, cortical amygdalar area, posterior part; CP, caudoputamen; DG, dentate gyrus; ECT, ectorhinal area; Ent, entorhinal cortex; EPd, endopiriform nucleus; HIP, hippocampus; HY, hypothalamus; MB, midbrain; MOp, primary motor area; MOs, secondary motor area; NLOT, nucleus of the lateral olfactory tract; ORBl, lateral orbital area; OT, olfactory tubercle; PERI, perirhinal area; Pir, piriform cortex; PL/ILA, prelimbic and infralimbic cortices; RSP, retrosplenial area; SSp, primary somatosensory area; TEa, temporal association area; THd, dorsal thalamic areas; TTd, dorsal taenia tecta.

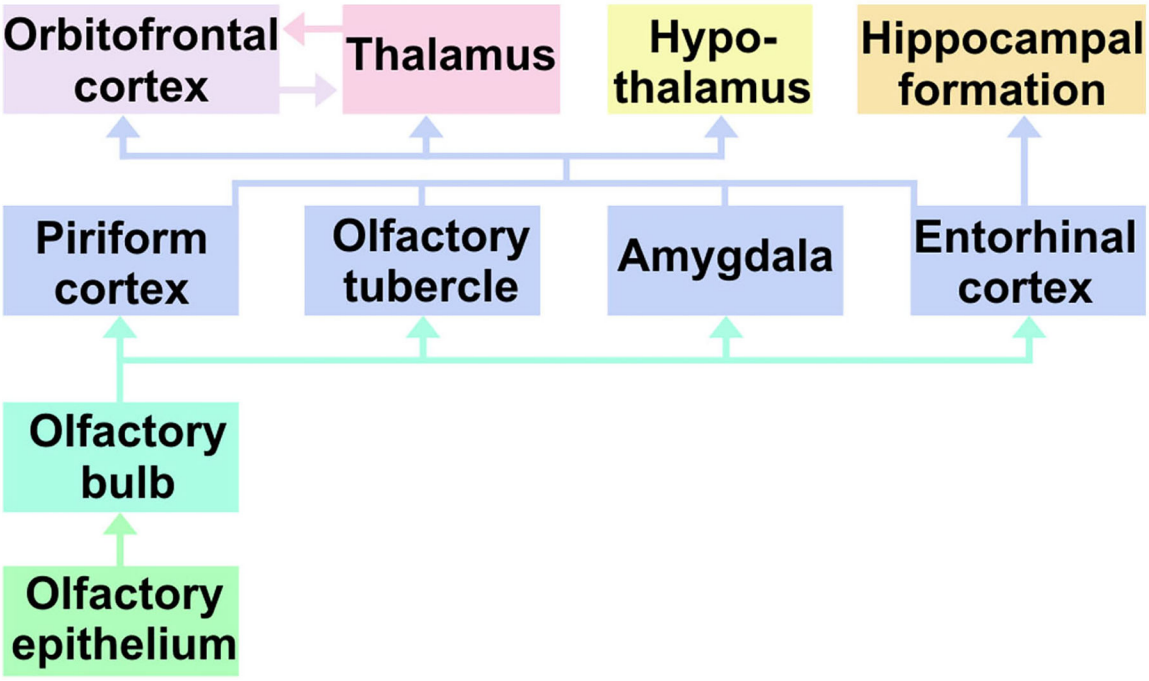

Fig. 3.
A schematic representation of olfactory system connections.

Table 1

Z-Scores of major brain regions activated by either IAA or mouse urine. The ROI volume and activated volumes (Z > 2.3) are given.

Structure	ROI Volume (mm^3)	IAA		Urine	
		Z mean	Volume (mm^3)	Z mean	Volume (mm^3)
ORBl	3.19	2.1	1.27	2.2	1.56
EPd	0.94	5.4	0.94	1.8	0.27
ILA	1.50	0.9	0.27	2.6	0.92
PL	1.77	−0.2	0.03	2.6	1.20
Pir	9.87	5.3	9.76	1.5	1.82
ACAv	1.97	0.0	0.0	2.4	1.19
OT	3.77	3.1	2.49	0.8	0.09
HY	14.29	0.5	0.17	1.4	2.68
NLOT	0.42	4.9	0.39	0.6	0.0
COAa	0.31	5.1	0.30	0.7	0.0

ACAv ventral part of anterior cingulate area; COAa, cortical amygdalar area, anterior part; EPd, endopiriform nucleus; HY, hypothalamus; ILA, infralimbic area; NLOT, nucleus of the lateral olfactory tract; ORBl, lateral orbital area; OT, olfactory tubercle; Pir, piriform cortex; PL, prelimbic area.